ACS OMEGA

http://pubs.acs.org/journal/acsodf

Article

# Synthesis, Characterization, and Investigation of the Antimicrobial Activity of Cetylpyridinium Tetrachlorozincate

Viktor Dubovoy, Shiri Nawrocki, Gaurav Verma, Lukasz Wojtas, Primit Desai, Hassan Al-Tameemi, Tatiana V. Brinzari, Michael Stranick, Dailin Chen, Shaopeng Xu, Shengqian Ma, Jeffrey M. Boyd, Tewodros Asefa, and Long Pan*

Cite This: *ACS Omega* 2020, 5, 10359−10365

Read Online

ACCESS | Metrics & More | Article Recommendations | Supporting Information

**ABSTRACT:** Cetylpyridinium tetrachlorozincate (referred to herein as $(CP)_2ZnCl_4$) was synthesized and its solid-state structure was elucidated *via* single-crystal X-ray diffraction (SC-XRD), revealing a stoichiometry of $C_{42}H_{76}Cl_4N_2Zn$ with two cetylpyridinium (CP) cations per $[ZnCl_4]^{2-}$ tetrahedra. Crystal structures at 100 and 298 K exhibited a zig-zag pattern with alternating alkyl chains and zinc units. The material showed potential for application as a broad-spectrum antimicrobial agent, to reduce volatile sulfur compounds (VSCs) generated by bacteria, and in the fabrication of advanced functional materials. Minimum inhibitory concentration (MIC) of $(CP)_2ZnCl_4$ was 60, 6, and 6 $\mu g\ mL^{-1}$ for *Salmonella enterica*, *Staphylococcus aureus*, and *Streptococcus mutans*, respectively. The MIC values of $(CP)_2ZnCl_4$ were comparable to that of pure cetylpyridinium chloride (CPC), despite the fact that approximately 16% of the bactericidal CPC is replaced with bacteriostatic $ZnCl_2$ in the structure. A modified layer-by-layer deposition technique was implemented to synthesize mesoporous silica (*i.e.*, SBA-15) loaded with approximately 9.0 wt % CPC and 8.9 wt % Zn.

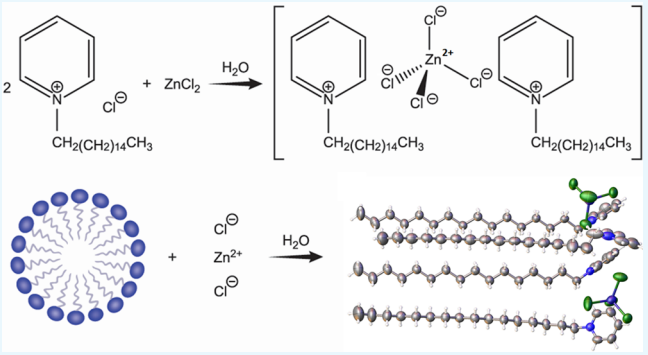


## INTRODUCTION

Cetylpyridinium chloride (CPC) is a quaternary ammonium compound with broad-spectrum antimicrobial activity. Its antimicrobial properties render it useful in a variety of applications including cosmetics, pharmaceuticals, and water treatment.[1,2] CPC is recognized as safe for dermal and oral applications by the Food and Drug Administration (FDA) and is commonly known for its role in the prevention and treatment of dental plaque, gingivitis, halitosis, and calculus in oral care products.[1,3−7] Zinc (Zn) is utilized in a wide array of industries including food, pharmaceuticals, energy production, material science, physiology, and organic chemistry.[8−11] Existing exclusively as the divalent Zn cation, Zn is an essential nutrient for virtually all living organisms.[12] However, at concentrations higher than those that are physiologically useful, Zn exhibits a bacteriostatic effect on many microorganisms.[13]

The antibacterial property of $Zn^{2+}$ ions has been attributed to five main mechanisms: (1) the disruption of cell membrane integrity, (2) the denaturation of proteins, (3) the production of reactive oxygen species resulting in cellular damage, (4) the interaction with nucleic acids, and (5) the inactivation of iron−sulfur proteins and/or inhibition of the iron−sulfur protein maturation machinery.[14−18] When CPC disrupts the microbial cell membrane, the positively charged region of CPC binds directly to the polar negatively charged phosphate groups of phospholipids while the nonpolar portion of CPC interacts with nonpolar phospholipid tails.[3,19] This results in the permeability of the cell membrane, membrane depolarization, leakage of intracellular components, and ultimately death.[3] Recent experiments suggest that loading quaternary ammonium compounds (QACs) into mesoporous silica nanoparticles (MSNs) yields a material with excellent antimicrobial activity and a pH-responsive controlled release of the antimicrobial drug.[20]

Previously, a number of studies have focused on elucidating the interaction between divalent metal (*e.g.*, Cd, Cu, and Zn) ions and pyridine analogues; however, these studies were not successful in identifying and realizing an antibacterial technology that is viable, safe, and effective for widespread healthcare use. In 2002, Neve *et al.* synthesized and solved the crystal structure of $[C16\text{-}Py]_2[CdCl_4]$.[21] The application of the material was not evaluated or mentioned beyond its potential

**Received:** January 10, 2020
**Accepted:** April 9, 2020
**Published:** April 28, 2020

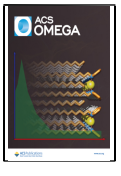

to be used as a liquid-crystalline precursor. Furthermore, attempts to crystallize the Zn analog were futile. Hilp *et al.* proposed the use of cetylpyridinium tetrachlorozincate as a titrant for analysis of anionic surfactants.[22,23] In 2015, Kaur *et al.* synthesized $(CP)_2CuCl_4$ and $(CP)CuCl_3$ and demonstrated that the insertion of copper into the CPC moiety enhanced the antibacterial activity as compared to pure CPC.[24] Although the antimicrobial properties of copper (Cu) have long been known, the realization of the Cu−cetylpyridinium conjugate technology for healthcare applications would be extremely challenging due to the potential for blue (*e.g.*, $Cu^{2+}$) or yellow (*e.g.*, $[CP][CuCl_3]$ or $[CP]_2[CuCl_4]$) staining associated with the d-orbital splitting of the copper ion.

The current work reports the synthesis and characterization of cetylpyridinium tetrachlorozincate as well as its application to reduce volatile sulfur compounds, as an antibacterial active pharmaceutical ingredient (API), and to fabricate advanced functional materials. Work presented suggests that cetylpyridinium tetrachlorozincate is a viable and effective antimicrobial agent to combat the global healthcare issues associated with oral and dermal disease (*e.g.*, hospital infections, medical device biofilms, and antibiotic resistance).

## RESULTS AND DISCUSSION

Initial observation of an interaction between CPC and $ZnCl_2$ was made while attempting to synthesize a deep eutectic solvent *via* anhydrous route. In particular, monohydrate CPC and anhydrous $ZnCl_2$ powders were combined, mixed, and heated at 90 °C for 24 h. Under these conditions, a translucent, yellow-colored gel material was formed in samples with a Zn/CPC ratio of 2 and higher. The material would undergo a phase change below approximately 50 °C to form an off-white opaque solid material. To improve the homogeneity of the samples, the synthesis was repeated with the addition of 15% water. Subsequent experiments, aimed to develop an aqueous route for the synthesis, demonstrated that a sparingly water-soluble precipitate is formed upon a combination of aqueous CPC and $ZnCl_2$ solutions above a certain threshold concentration. The solubility of the precipitate in water was <1 wt % at room temperature. The precipitate was collected, washed with copious amounts of water, and recrystallized from acetone to yield a single crystal adequate for single-crystal X-ray diffraction (SC-XRD) analysis. Dynamic scanning calorimetry (DSC) experiments (Figure S1) demonstrated a ∼20 °C reduction in the onset temperature of the endothermic melting peak in the synthesized material as compared to pure CPC. These results are consistent with the observed phase transition below approximately 50 °C in the gel samples synthesized *via* anhydrous route.

X-ray photoelectron spectroscopy (XPS) and Fourier-transform infrared (FTIR) spectroscopy were used to confirm complex formation prior to SC-XRD analyses and therefore referred to as the CPC−Zn material. The XPS results (Figures S2 and S3) indicate that there is a slight shift in the $N^+$ peak for the CPC−Zn (402.2 eV) material as compared to the CPC (401.8 eV) reference. This may indicate that the electronic environment around the cationic N in the CPC part of the sample has changed as compared to that in CPC alone. It is noteworthy that anhydrous $ZnCl_2$ cannot be easily analyzed by conventional XPS and FTIR due to its hygroscopic properties.

The FTIR spectra of $CPC{\cdot}H_2O$, $ZnCl_2$, and as-synthesized CPC−Zn material are shown in Figure 1. The spectrum of the CPC−Zn sample clearly shows the fingerprint of the

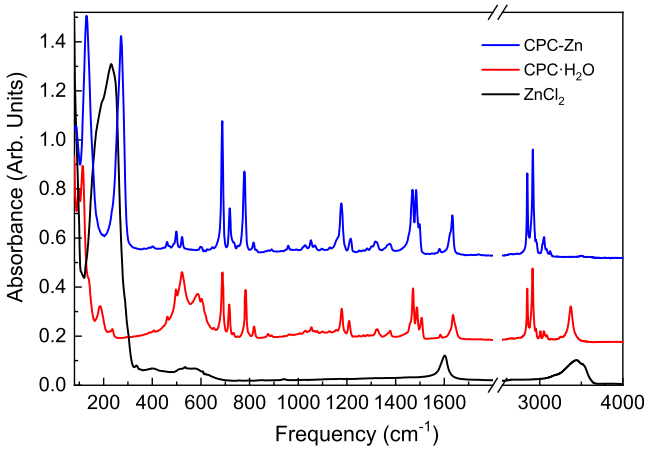


**Figure 1.** Infrared absorption spectrum of the synthesized CPC−Zn material in comparison to the $CPC{\cdot}H_2O$ and $ZnCl_2$ precursors. The spectra are offset for clarity.

cetylpyridinium, confirming its presence in the sample. A close inspection of the spectrum demonstrates, however, that the bands of cetylpyridinium in the CPC−Zn material do not match the pure $CPC{\cdot}H_2O$ compound. The majority of the bands related to C−H, $CH_2$, C−C, C═C, and C═N stretching and bending vibrations of cetylpyridinium display shifted peak positions as compared to the $CPC{\cdot}H_2O$ raw material.[25,26] The $\nu$(OH) peak at 3372 $cm^{-1}$ as well as another broad $H_2O$-related band near 550 $cm^{-1}$ seen in the $CPC{\cdot}H_2O$ starting compound have also disappeared in the presence of Zn. Furthermore, a distinguishable new peak at 272 $cm^{-1}$ is evident in the CPC−Zn sample, likely originating from the ZnCl-related vibration. Taken together, the FTIR data indicate that the interaction of cetylpyridinium chloride with $ZnCl_2$ resulted in the formation of a new complex.

To elucidate the structure of the complex and analyze the interactions involved, SC-XRD analysis was carried out which shows that the coordination complex crystallizes in the orthorhombic *Pbca* space group. The structural formula can be described as $[(C_{21}H_{38}N)_2][ZnCl_4]$, or $(CP)_2ZnCl_4$ for short, whereby two $ZnCl_4^{2-}$ units are present in close contact with four cetylpyridinium units by C−H−Cl interactions (Figure 2). The packing behavior is depicted in Figure 3. As seen from the structure, the alkyl chain units and the Zn units pack in a zig-zag manner, with each unit present at alternating ends.

The crystals contain a disordered solvent that was modeled as a $H_2O$ molecule (atom O1). It was not possible to locate the

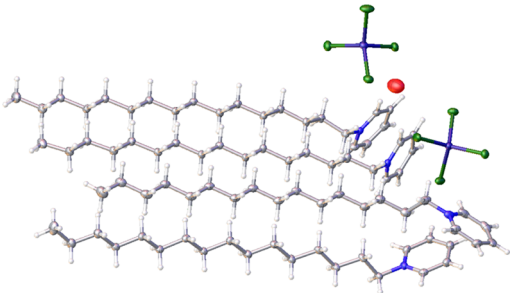

**Figure 2.** Structure of $[(C_{21}H_{38}N)_2][ZnCl_4]$, illustrating carbon (gray), hydrogen (white), nitrogen (blue), zinc (purple), chloride (green), and oxygen (red) atoms.



https://dx.doi.org/10.1021/acsomega.0c00131
*ACS Omega* 2020, 5, 10359−10365

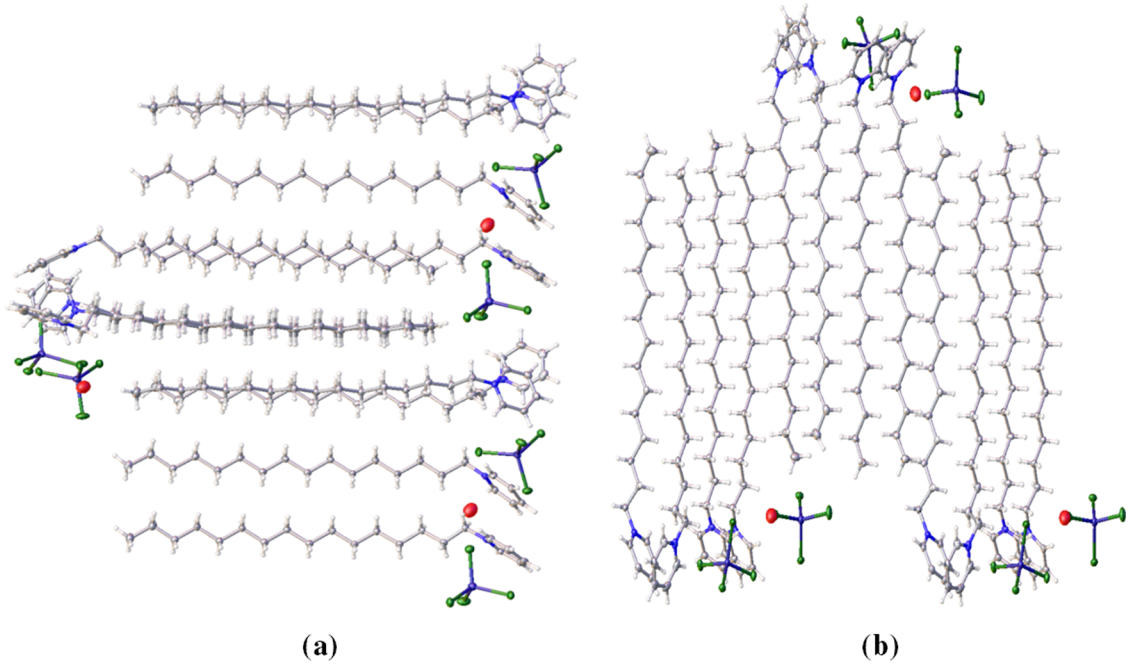


**Figure 3.** Packing of $[(C_{21}H_{38}N)_2][ZnCl_4]$ along (a) (110) plane and (b) (100) plane.

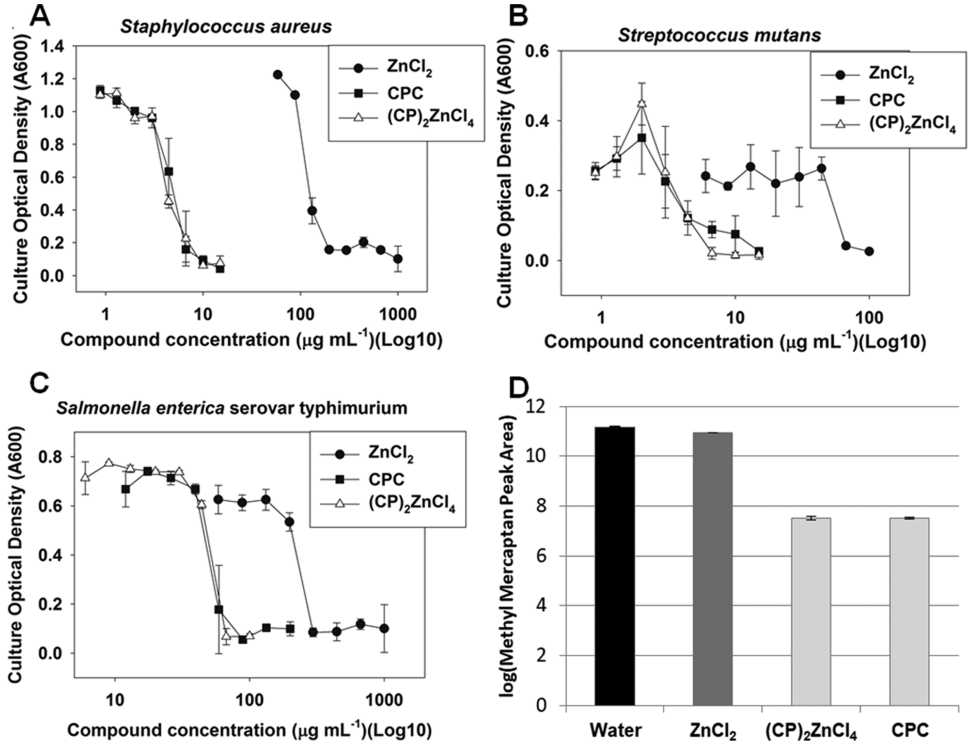


**Figure 4.** Inhibition of *Staphylococcus aureus* (A), *Streptococcus mutans* (B), and *Salmonella enterica* (C) with $ZnCl_2$, CPC, and $(CP)_2ZnCl_4$. VSC reduction efficacy (D) of methyl mercaptan with color shading corresponding to the statistical group (Table S4).

hydrogen atoms of $H_2O$. The occupancy of the $H_2O$ molecule is ~0.25 and it is not present in the crystals collected at room temperature (Figure S5). There is a structural change with the increase in temperature and concomitant loss of the solvent $H_2O$ molecule. The distance between the Zn(II) centers (Zn01−Zn02) increases from 8.73 Å (at 100 K) to 9.05 Å (at 298 K). However, the packing behavior at room temperature remains similar in a zig-zag manner (Figure S5).

The effect of $ZnCl_2$, $(CP)_2ZnCl_4$, and CPC on in vitro bacteria-generated volatile sulfur compounds (VSC), conducted by methyl mercaptan gas chromatography (GC) headspace measurement, is illustrated in Figure 4D. Statistical grouping, calculated using the Tukey method and a 95.0% confidence interval, indicates that CPC and $(CP)_2ZnCl_4$ exhibit parity efficacy for malodor-causing VSCs.[27] However, at the measured concentration, $ZnCl_2$ exhibits a weak VSC reduction effect as compared to CPC and $(CP)_2ZnCl_4$. The


https://dx.doi.org/10.1021/acsomega.0c00131
ACS Omega 2020, 5, 10359−10365

elemental composition of the powders evaluated for VSC reduction is shown in Table S3. The concentration of $ZnCl_2$ (*i.e.*, 16.22 wt %) in the $(CP)_2ZnCl_4$ is in decent agreement with the theoretical value (*i.e.*, 16.70 wt %), which implies adequate purity of the sample as a result of the acetone extraction process.

The ability of CPC, Zn, and $(CP)_2ZnCl_4$ to inhibit the growth of bacterial pathogens (*i.e.*, *Staphylococcus aureus* LAC, *S. mutans*, and *S. enterica* Serovar typhimurium) was examined. *S. aureus* LAC is a Gram-positive community-associated methicillin-resistant CA-MRSA strain and a representative strain of the USA300 clone, which is a leading cause of skin and soft tissue infections in North America.[28,39] *S. mutans* is also Gram positive and the leading causes of dental caries.[29] *S. enterica* Serovar typhimurium is Gram negative and a primary enteric pathogen affecting humans.[30,40]

The minimal inhibitory concentrations of CPC, Zn, and $(CP)_2ZnCl_4$ were determined in liquid culture after static growth. All of the three bacteria displayed typical dose–responses to the compounds utilized (Figure 4A–C). The MICs for Zn for *S. aureus*, *S. enterica*, and *S. mutans* were approximately 200, 300, and 65 $\mu g\ mL^{-1}$, respectively. The MICs of $(CP)_2ZnCl_4$ for *S. aureus*, *S. enterica*, and *S. mutans* were 6, 60, and 6 $\mu g\ mL^{-1}$, respectively. The MICs for CPC were similar to those for $(CP)_2ZnCl_4$ in the case of *S. aureus* and *S. enterica*. In the case of *S. mutans*, a slight improvement in the antimicrobial activity was demonstrated for $(CP)_2ZnCl_4$; however, the results did not reach statistical significance.

A previous work demonstrated that the utilization of MSNs as drug delivery vehicles for QACs yields a material with a pH-responsive controlled drug release as well as excellent antimicrobial activity.[20] Herein, the feasibility of incorporating $(CP)_2ZnCl_4$ into such drug delivery systems (DDSs), where the surface of MSNs can be further modified to impart selectivity or other advantages, was explored.[31] The material where $(CP)_2ZnCl_4$ was loaded into SBA-15 MSNs is referred to as CPC–Zn@SBA-15 henceforth due to a certain amount of uncertainty whether all CPC–Zn moieties within the MSNs are in fact $(CP)_2ZnCl_4$. Actually, the elemental composition suggests an excess of Zn, which is likely chemisorbed to the silanol groups. Bulk elemental composition measurements of CPC–Zn@SBA-15 were conducted using thermogravimetric analysis (TGA) and inductively coupled plasma optical emission spectroscopy (ICP-OES) for CPC (9.0 wt %) and Zn (8.9 wt %), respectively. XPS analysis was conducted on mesoporous SBA-15, CPC@SBA-15, and CPC–Zn@SBA-15 to probe the elemental composition near the surface of the MSNs. Calcined SBA-15 is consistent with the composition of silica with a surface that is essentially free (1.1 wt % C) from organic contamination. The $N^+$/Cl ratio (1.29) of the CPC@SBA-15 sample suggests that a portion of the cetylpyridinium cations has been adsorbed onto the negative silanol groups of silica. The $N^+$ binding energy is shifted slightly relative to the CPC reference, while the Cl binding energy is significantly shifted relative to CPC. This implies that both $N^+$ and Cl are in different chemical bonding environments on the silica surface, compared to bulk CPC. The surface of the CPC–Zn@SBA-15 material exhibited 3.36 wt % Zn, 1.01 wt % CPC, and a Zn/CPC ratio of 3.33. The Zn/CPC ratio indicates that $(CP)_2ZnCl_4$ is present on the surface with excess $ZnCl_2$. Since the sample was washed with water after preparation, it is possible that the $(CP)_2ZnCl_4$ recrystallized on the surface or dissolved into its ionic constituents and precipitated onto the surface of MSNs.

As discussed above, ICP-OES, TGA, and XPS analyses demonstrate significant amounts of cetylpyridinium and Zn in the CPC–Zn@SBA-15 sample. FTIR was further used to investigate the presence of $(CP)_2ZnCl_4$ within the silica framework. Figure S9 shows the spectrum of the CPC–Zn@SBA-15 sample in comparison to the CPC@SBA-15 control and the SBA-15 mesoporous silica. SBA-15 displays a typical silica spectrum with asymmetric and symmetric $\nu$(Si–O) vibrations near 1060 and 800 $cm^{-1}$, respectively, nonbridging $\nu(Si–O^-)$ stretching vibration and/or $\nu$(Si–OH) vibration of silanol groups near 955 $cm^{-1}$, and $\delta$(O–Si–O) bending modes around 440 $cm^{-1}$. The absorption spectra of CPC–Zn@SBA-15 and CPC@SBA-15 support the presence of cetylpyridinium in both samples as evident from its characteristic vibrations near 1500 $cm^{-1}$ region as well as near the $\nu$(C–H) stretching band region where two peaks around 2855 and 2925 $cm^{-1}$ corresponding to symmetric and asymmetric $\nu(CH_2)$ vibrations are observed.[34] Importantly, in addition to cetylpyridinium bands, the CPC–Zn@SBA-15 sample exhibits two distinct peaks near 115 and 295 $cm^{-1}$, in line with the pure $(CP)_2ZnCl_4$ profile that displays two strong bands below 300 $cm^{-1}$ (Figure 1). This finding suggests the presence of the $(CP)_2ZnCl_4$ complex on the silica surface. Note, the peak positions of cetylpyridinium and $(CP)_2ZnCl_4$ incorporated into silica are shifted as compared to their bulk constituents. The latter may be attributed to adsorption and/or confinement effects.

## CONCLUSIONS

A novel CPC complex, cetylpyridinium tetrachlorozincate, was synthesized and unambiguously characterized *via* single-crystal X-ray diffraction (SC-XRD) measurements, indicating a stoichiometry of $C_{42}H_{76}Cl_4N_2Zn$ with two cetylpyridinium cations per $[ZnCl_4]^{2-}$ tetrahedra. The material was evaluated and shows promising characteristics for application as a broad-spectrum antimicrobial agent, to reduce volatile sulfur compounds (VSCs) generated by bacteria, and in the synthesis of advanced functional materials. VSC experiments and antimicrobial assays demonstrate that $(CP)_2ZnCl_4$ exhibits at least parity efficacy to pure CPC while comprising approximately 16% of the significantly less efficacious and expensive zinc chloride material. An advanced functional material was prepared by successfully loading $(CP)_2ZnCl_4$ into SBA-15, which is a promising candidate for a highly efficient drug delivery system (DDS) for stimulated-release antimicrobial applications.[20,35] This new technology paves the way for the development of next generation and highly efficacious healthcare treatments with potentially reduced risk of exacerbating the problem of antibiotic resistance.

## EXPERIMENTAL SECTION

**Synthesis of $(CP)_2ZnCl_4$.** Reagent-grade anhydrous zinc chloride ($ZnCl_2$) and cetylpyridinium chloride monohydrate were supplied by Sigma-Aldrich (St. Louis, MO). All materials were used as-is without further purification. The synthesis entailed preparation of fresh 25 wt % CPC and 75 wt % zinc chloride solutions in deionized water. Subsequently, the $ZnCl_2$ solution was added dropwise to the CPC solution under magnetic stirring. Vacuum filtration and drying of the precipitate yielded an off-white solid, which was further


https://dx.doi.org/10.1021/acsomega.0c00131
ACS Omega 2020, 5, 10359–10365

purified using acetone extraction. A single crystal was obtained by recrystallizing from acetone.

**Characterization.** X-ray photoemission spectroscopy (XPS) analysis was carried out using a PHI 5000 VersaProbe II scanning XPS microprobe instrument with a monochromatic Al K$\alpha$ X-ray source (1486.6 eV) and 200 $\mu$m beam diameter. PHI MultiPak software was used for subsequent data analysis. Fourier-transform infrared (FTIR) spectra were collected using a Bruker Vertex 70 FTIR spectrometer (Bruker Optics, Billerica, MA) equipped with a GladiATR diamond ATR accessory (Pike Technologies, Madison, WI). The spectral range was 80−4000 $cm^{-1}$ and a resolution of 4 $cm^{-1}$ was used. All measurements were carried out at room temperature, using as-prepared powder samples, without any additional sample preparation procedures. The single-crystal X-ray diffraction (SC-XRD) data were collected using Bruker D8 Venture PHOTON 100 CMOS system equipped with a Cu K$\alpha$ INCOATEC ImuS microfocus source ($\lambda$ = 1.54178 Å). Powder X-ray diffraction (PXRD) data were collected at room temperature using a Bruker D8 Advance $\theta$−$2\theta$ diffractometer with copper radiation (Cu K$\alpha$, $\lambda$ = 1.5406 Å) and a secondary monochromator operating at 40 kV and 40 mA, whereby samples were measured in the $2\theta$ range of 2 to 40° at 0.5 s/step and a step size of 0.02°. Small-angle X-ray scattering (SAXRD) patterns were obtained by using a Bruker Vantec-500 area detector and a Bruker FR571 rotating-anode X-ray generator operating at 40 kV and 50 mA. The diffraction system was equipped with a 3-circle Azlan goniometer, but the sample was not moved during X-ray data collection. The system used 0.25 mm pinhole collimation and a Rigaku Osmic parallel-mode (*e.g.*, primary beam dispersion less than 0.01° in $2\theta$) mirror monochromator (Cu K$\alpha$, $\lambda$ = 1.5418 Å). Data were collected at room temperature (~20 °C) with a sample to detector distance of 26.25 cm. Spatial calibration and flood-field correction for the area detector were performed at this distance prior to data collection. The 2048 × 2048 pixel images were collected at the fixed detector ($2\theta$) angle of 50° for 600 s with $\omega$ step of 0.00°. For the intensity versus $2\theta$ plot, a 0.02° step, bin-normalized $\chi$ integration was performed on the general area detector diffraction system (GADDS) frame image. Brunauer−Emmett−Teller (BET) surface area and porosity measurements of the SBA-15 mesoporous silica nanoparticles (MSNs) were evaluated using a Surface Area and Porosity Analyzer (Gemini VII, Micromeritics).[36] Samples were outgassed at 100 °C overnight under a constant flow of $N_2$. Subsequent adsorption−desorption measurements were done at 77 K. Barrett−Joyner−Halenda (BJH) analysis was used to determine pore size distribution.[37] Volatile sulfur compound measurements and antimicrobial assays are described in detail in the Supporting Information.[38−41] (Table 1)[38−4138−41]

**Synthesis of SBA-15.** Pluronic P123, 34% hydrochloric acid, and tetraethyl orthosilicate (TEOS) were supplied by BASF (Ludwigshafen, Germany), Avantor (Allentown, PA), and Sigma-Aldrich (St. Louis, MO), respectively. All materials were used as received without further purification. Santa Barbara Amorphous (SBA-15)-type material was synthesized according to conventional methods. Specifically, 4 g of pluronic P123 was mixed with 104 mL of water and 24 mL of concentrated hydrochloric acid. To this clear solution, 8.53 g of TEOS was added dropwise and subsequently stirred at 40 °C for 24 h. The resulting white powder was filtered, washed with copious amounts of deionized water, and dried at 50 °C overnight. Calcination of the as-synthesized SBA-15 was conducted in air at 550 °C for 6 h with 10 °C/min. Cetylpyridinium chloride tetrachlorozincate was incorporated into the SBA-15 framework *via* a modified immersion layer-by-layer deposition technique.[42] After outgassing the SBA-15 at 100 °C for 2 h under vacuum, 800 mg of the powder was added to 100 g of 10 wt % aqueous CPC solution with subsequent magnetic stirring for over 1 h to allow diffusion throughout the porous framework. The CPC-containing SBA-15 was centrifuged, filtered, and washed with 150 mL of deionized water. Finally, the powder was washed with 100 g of 10 wt % $ZnCl_2$ aqueous solution, washed with 150 mL of deionized water, and dried at 40 °C under vacuum for several days. It is noteworthy that the utilization of higher concentrations of CPC and $ZnCl_2$ solutions failed to yield homogeneous CPC−Zn@SBA-15 powders. SBA-15 was chosen as the porous framework since its pore width can easily accommodate a CPC molecule.

**Table 1. Porosimetry Results and SAXRD Data**

| sample | BET surface area ($m^2$/g) | pore width (Å) | pore wall thickness (Å) | 2$\theta$ | crystal size[a] (nm) |
|---|---|---|---|---|---|
| SBA-15 | 627 | 48 | 18 | 1.328 | 77 |
| CPC@ SBA-15 | 153 | 45 | | | |
| CPC−Zn@ SBA-15 | 90 | 43 | | 1.311 | 66 |

[a]Crystallite size obtained using the Scherrer equation.[32,33]

## ■ ASSOCIATED CONTENT

### Supporting Information

The Supporting Information is available free of charge at https://pubs.acs.org/doi/10.1021/acsomega.0c00131.

Colgate_CetylpyZn_Acetone_100 K (CIF)
Colgate_CetylpyZn_Acetone_298 K (CIF)
General procedure for volatile sulfur compound (VSC) measurements, antimicrobial assays, and supplemental characterization of $(CP)_2ZnCl_4$ (PDF)

## ■ AUTHOR INFORMATION


### Corresponding Author

**Long Pan** − *Colgate-Palmolive Company, Piscataway, New Jersey 08854, United States;* orcid.org/0000-0003-0438-4040; Email: longyuepan@yahoo.com

### Authors

**Viktor Dubovoy** − *Department of Chemistry and Chemical Biology, Rutgers, The State University of New Jersey, Piscataway, New Jersey 08854, United States*

**Shiri Nawrocki** − *Department of Medicine, Rutgers Robert Wood Johnson Medical School, Piscataway, New Jersey 08854, United States*

**Gaurav Verma** − *Department of Chemistry, University of South Florida, Tampa, Florida 33620, United States*

**Lukasz Wojtas** − *Department of Chemistry, University of South Florida, Tampa, Florida 33620, United States*

**Primit Desai** − *Department of Biochemistry and Microbiology, Rutgers, The State University of New Jersey, New Brunswick, New Jersey 08854, United States*




https://dx.doi.org/10.1021/acsomega.0c00131
ACS Omega 2020, 5, 10359−10365

**Hassan Al-Tameemi** − *Department of Biochemistry and Microbiology, Rutgers, The State University of New Jersey, New Brunswick, New Jersey 08854, United States*
**Tatiana V. Brinzari** − *Colgate-Palmolive Company, Piscataway, New Jersey 08854, United States*
**Michael Stranick** − *Colgate-Palmolive Company, Piscataway, New Jersey 08854, United States*
**Dailin Chen** − *Colgate-Palmolive Company, Guangzhou 510620, China*
**Shaopeng Xu** − *Colgate-Palmolive Company, Guangzhou 510620, China*
**Shengqian Ma** − *Department of Chemistry, University of South Florida, Tampa, Florida 33620, United States;* orcid.org/0000-0002-1897-7069
**Jeffrey M. Boyd** − *Department of Biochemistry and Microbiology, Rutgers, The State University of New Jersey, New Brunswick, New Jersey 08854, United States*
**Tewodros Asefa** − *Department of Chemistry and Chemical Biology and Department of Chemical and Biochemical Engineering, Rutgers, The State University of New Jersey, Piscataway, New Jersey 08854, United States;* orcid.org/0000-0001-8634-5437

Complete contact information is available at: https://pubs.acs.org/10.1021/acsomega.0c00131

### Author Contributions

The manuscript was written through the contributions of all authors.

### Funding

NIAID award 1R01AI139100-01 from the National Institutes of Health.

### Notes

The authors declare no competing financial interest.

## ■ ACKNOWLEDGMENTS

The authors would like to thank Dr. Thomas Emge and Dr. Chi-yuan Cheng for their assistance in X-ray diffraction and nuclear magnetic resonance, respectively. The Boyd lab is funded by NIAID award 1R01AI139100-01 from the National Institutes of Health.

## ■ REFERENCES

(1) Ash, M.; Ash, I. *Handbook of Preservatives*; Synapse Information Resources, 2004.
(2) Imai, H.; Kita, F.; Ikesugi, S.; Abe, M.; Sogabe, S.; Nishimura-Danjobara, Y.; Miura, H.; Oyama, Y. Cetylpyridinium chloride at sublethal levels increases the susceptibility of rat thymic lymphocytes to oxidative stress. *Chemosphere* **2017**, *170*, 118−123.
(3) US Department of Health and Human Services. Oral health care drug products for over-the-counter human use; antigingivitis/antiplaque drug products; establishment of a monograph; proposed rules. *Fed. Regist.* **2003**, *68*, 32247−32287.
(4) Sreenivasan, P. K.; Haraszthy, V. I.; Zambon, J. J. Antimicrobial efficacy of 0.05% cetylpyridinium chloride mouthrinses. *Lett. Appl. Microbiol.* **2013**, *56*, 14−20.
(5) Liu, J.; Ling, J.-Q.; Wu, C. D. Cetylpyridinium chloride suppresses gene expression associated with halitosis. *Arch. Oral Biol.* **2013**, *58*, 1686−1691.
(6) Witt, J.; Ramji, N.; Gibb, R.; Dunavent, J.; Flood, J.; Barnes, J. Antibacterial and antiplaque effects of a novel, alcohol-free oral rinse with cetylpyridinium chloride. *J. Contemp. Dent. Pract.* **2005**, *6*, 001−009.
(7) Rahardjo, A.; Ramadhani, A.; Adiatman, M.; Wimardhani, Y. S.; Maharani, D. A. Efficacy of Mouth Rinse Formulation Based On Cetyl Pyridinium Chloride in the Control of Plaque as an Early Onset of Dental Calculus Built Up. *J. Int. Dent. Med.* **2016**, *9*, 184−188.
(8) Crans, D. C.; Meade, T. J. Preface for the forum on metals in medicine and health: new opportunities and approaches to improving health. *Inorg. Chem.* **2013**, *52*, 12181−12183.
(9) Martin, D. P.; Hann, Z. S.; Cohen, S. M. Metallo-protein-inhibitor binding: human carbonic anhydrase II as a model for probing metal-ligand interactions in a metalloprotein active site. *Inorg. Chem.* **2013**, *52*, 12207−12215.
(10) Wu, X.-F.; Neumann, H. Zinc-Catalyzed Organic Synthesis: C-C, C-N, C-O Bond Formation Reactions. *Adv. Synth. Catal.* **2012**, *354*, 3141−3160.
(11) Mainar, A. R.; Iruin, E.; Colmenares, L. C.; Kvasha, A.; de Meatza, I.; Bengoechea, M.; Leonet, O.; Boyano, I.; Zhang, Z.; Blazquez, J. A. An overview of progress in electrolytes for secondary zinc-air batteries and other storage systems based on zinc. *J. Energy Storage* **2018**, *15*, 304−328.
(12) Ma, L.; Terwilliger, A.; Maresso, A. W. Iron and zinc exploitation during bacterial pathogenesis. *Metallomics* **2015**, *7*, 1541−1554.
(13) Chandrangsu, P.; Rensing, C.; Helmann, J. D. Metal homeostasis and resistance in bacteria. *Nat. Rev. Microbiol.* **2017**, *15*, 338−350.
(14) Stanić, V.; Dimitrijević, S.; Antić-Stanković, J.; Mitrić, M.; Jokić, B.; Plećaš, I. B.; Raičević, S. Synthesis, characterization and antimicrobial activity of copper and zinc-doped hydroxyapatite nanopowders. *Appl. Surf. Sci.* **2010**, *256*, 6083−6089.
(15) Zhang, J.; Qin, X.; Wang, B.; Xu, G.; Qin, Z.; Wang, J.; Wu, L.; Ju, X.; Bose, D. D.; Qiu, F.; Zhou, H.; Zou, Z. Zinc oxide nanoparticles harness autophagy to induce cell death in lung epithelial cells. *Cell Death Dis.* **2017**, *8*, No. e2954.
(16) Pasquet, J.; Chevalier, Y.; Pelletier, J.; Couval, E.; Bouvier, D.; Bolzinger, M.-A. The contribution of zinc ions to the antimicrobial activity of zinc oxide. *Colloids Surf., A* **2014**, *457*, 263−274.
(17) Li, J.; Ren, X.; Fan, B.; Huang, Z.; Wang, W.; Zhou, H.; Lou, Z.; Ding, H.; Lyu, J.; Tan, G. Zinc Toxicity and Iron-Sulfur Cluster Biogenesis in *Escherichia coli*. *Appl. Environ. Microbiol.* **2019**, *85*, No. e01967-18.
(18) Xu, F. F.; Imlay, J. A. Silver(I), Mercury(II), Cadmium(II), and Zinc(II) Target Exposed Enzymic Iron-Sulfur Clusters when They Toxify *Escherichia coli*. *Appl. Environ. Microbiol.* **2012**, *78*, 3614−3621.
(19) Arrigler, V.; Kogej, K.; Majhenc, J.; Svetina, S. Interaction of cetylpyridinium chloride with giant lipid vesicles. *Langmuir* **2005**, *21*, 7653−7661.
(20) Dubovoy, V.; Ganti, A.; Zhang, T.; Al-Tameemi, H.; Cerezo, J. D.; Boyd, J. M.; Asefa, T. One-Pot Hydrothermal Synthesis of Benzalkonium-Templated Mesostructured Silica Antibacterial Agents. *J. Am. Chem. Soc.* **2018**, *140*, 13534−13537.
(21) Neve, F.; Francescangeli, O.; Crispini, A. Crystal architecture and mesophase structure of long-chain N-alkylpyridinium tetrachlorometallates. *Inorg. Chim. Acta* **2002**, *338*, 51−58.
(22) Hilp, M.; Zembatova, S. Cetylpyridinium tetrachlorozincate as standard for tenside titration. Analytical methods with 1,3-dibromo-5,5-dimethylhydantoin (DBH) in respect to environmental and economical concern, part 19. *Die Pharm.* **2004**, *59*, 615−617.
(23) Hilp, M. Determination of anionactive tensides using cetylpyridinium tetrachlorozincate as titrant. Analytical methods in respect to environmental and economical concern, part 20. *Die Pharm.* **2004**, *59*, 676−677.
(24) Kaur, G.; Kumar, S.; Dilbaghi, N.; Bhanjana, G.; Guru, S. K.; Bhushan, S.; Jaglan, S.; Hassan, P. A.; Aswal, V. K. Hybrid surfactants decorated with copper ions: aggregation behavior, antimicrobial activity and anti-proliferative effect. *Phys. Chem. Chem. Phys.* **2016**, *18*, 23961−23970.
(25) Gelmboldt, V. O.; Anisimov, V. Y.; Bevz, N. Y.; Georgiyants, V. A. Development of methods for identification of cetylpyridinium hexafluorosilicate. *Pharma Chem.* **2016**, *8*, 169−173.
(26) Cook, D. Vibrational Spectra of Pyridinium Salts. *Can. J. Chem.* **1961**, *39*, 2009−2024.

(27) Tukey, J. W. Comparing Individual Means in the Analysis of Variance. *Biometrics* **1949**, *5*, 99−114.
(28) Planet, P. J. Life After USA300: The Rise and Fall of a Superbug. *J. Infect. Dis.* **2017**, *215*, S71−S77.
(29) Loesche, W. J. Role of *Streptococcus mutans* in human dental decay. *Microbiol. Rev.* **1986**, *50*, 353.
(30) Fàbrega, A.; Vila, J. *Salmonella enterica* serovar Typhimurium skills to succeed in the host: virulence and regulation. *Clin. Microbiol. Rev.* **2013**, *26*, 308−341.
(31) Li, Z.; Barnes, J. C.; Bosoy, A.; Stoddart, J. F.; Zink, J. I. Mesoporous silica nanoparticles in biomedical applications. *Chem. Soc. Rev.* **2012**, *41*, 2590−2605.
(32) Scherrer, P. Bestimmung der Größe und der inneren Struktur von Kolloidteilchen mittels Röntgenstrahlen. *Nachr. Ges. Wiss. Gottingen* **1918**, *26*, 98−100.
(33) Langford, J. I.; Wilson, A. J. C. Scherrer after sixty years: A survey and some new results in the determination of crystallite size. *J. Appl. Crystallogr.* **1978**, *11*, 102−113.
(34) Kung, K. H. S.; Hayes, K. F. Fourier transform infrared spectroscopic study of the adsorption of cetyltrimethylammonium bromide and cetylpyridinium chloride on silica. *Langmuir* **1993**, *9*, 263−267.
(35) Yang, P.; Huang, S.; Kong, D.; Lin, J.; Fu, H. Luminescence functionalization of SBA-15 by $YVO_4$:$Eu^{3+}$ as a novel drug delivery system. *Inorg. Chem.* **2007**, *46*, 3203−3211.
(36) Brunauer, S.; Emmett, P. H.; Teller, E. Adsorption of Gases in Multimolecular Layers. *J. Am. Chem. Soc.* **1938**, *60*, 309−319.
(37) Barrett, E. P.; Joyner, L. G.; Halenda, P. P. The Determination of Pore Volume and Area Distributions in Porous Substances. I. Computations from Nitrogen Isotherms. *J. Am. Chem. Soc.* **1951**, *73*, 373−380.
(38) Yaegaki, K.; Sanada, K. Volatile sulfur compounds in mouth air from clinically healthy subjects and patients with periodontal disease. *J. Periodontal Res.* **1992**, *27*, 233−238.
(39) Roberts, C. A.; Al-Tameemi, H. M.; Mashruwala, A. A.; Rosario-Cruz, Z.; Chauhan, U.; Sause, W. E.; Torres, V. J.; Belden, W. J.; Boyd, J. M. The Suf Iron-Sulfur Cluster Biosynthetic System Is Essential in *Staphylococcus aureus*, and Decreased Suf Function Results in Global Metabolic Defects and Reduced Survival in Human Neutrophils. *Infect. Immun.* **2017**, *85*, No. e00100-17.
(40) Boyd, J. M.; Teoh, W. P.; Downs, D. M. Decreased Transport Restores Growth of a *Salmonella enterica* Mutant on Tricarballylate. *J. Bacteriol.* **2012**, *194*, 576−583.
(41) *Methods for Dilution Antimicrobial Susceptibility Tests for Bacteria That Grow Aerobically; Approved Standard*, 9th ed.; Clinical and Laboratory Standards Institute: Wayne, PA, 2012.
(42) Richardson, J. J.; Björnmalm, M.; Caruso, F. Technology-driven layer-by-layer assembly of nanofilms. *Science* **2015**, *348*, No. aaa2491.


https://dx.doi.org/10.1021/acsomega.0c00131
*ACS Omega* 2020, 5, 10359−10365